EasyChair Preprint

№ 6776

Investigation on Characteristics of Biogas Flameless Combustion in Asymmetric Combustor and Effect of Hydrogen Addition on Biogas Emission

Abdelgader Agilah Gheidan, Mazlan A. Wahid, Fudhail A Munir and Muhammad Amri Mazlan Wahid

October 6, 2021

Investigation on Characteristics of Biogas Flameless Combustion in Asymmetric Combustor and Effect of Hydrogen Addition on Biogas Emission

Abdelgader A.S. Gheidan[1, a)], Mazlan Bin Abdul Wahid[1, b)], Fudhail A Munir[2, c)], Amri Mazlan. A. Wahid[1,d])

[1]*High-Speed Reacting Flow Laboratory, School of Mechanical Engineering, Universiti Teknologi Malaysia, 81310 UTM Skudai, Johor, Malaysia*
[2]*Faculty of Mechanical Engineering, Universiti Teknikal Malaysia Melaka (UTeM), 76100 Durian Tunggal* Melaka, Malaysia

[a)] *Corresponding author:* E-mail: gheidan015@gmail.com
[b)]*mazzlan@utm.my*

Abstract. The world's energy demand has increased tremendously due to industrial development and population growth. The increased consumption of key energy sources such as coal, oil and natural gas has had a significant impact on the atmospheric environment. Of all alternative fuels, biogas offers the greatest potential benefit to the energy supply and the environment. Biogas from the anaerobic digestion of biomass and biological waste by microorganisms can be used in calefaction, transportation and power production as a sustainable energy supply. Nevertheless, the Low Calorific Value (LCV) of biogas poses a significant challenge for converting biogas into electrical or thermal energy. A three-dimensional (3D) CFD (Computational Fluid Dynamics) research was conducted to show the different arrangements of biogas flameless combustion compared to standard modes through using a computational methodology that impalements the Rε/k−ε and the eddy dissipation turbulence. Also, studying the effect of added hydrogen to the biogas composition from 2% to 8% by volume on NOx emissions. The findings validated flameless combustion as one of the leading methods for biogas usage. The decline in contaminant production and fuel consumption are the primary source of biogas flameless combustion dominance. Besides, adding only 2% of hydrogen to the biogas component leads to stability and uniform temperature, and adding hydrogen to the biogas component at up to 4% by volume alleviates the production of nitrogen oxides. However, adding hydrogen from 4% to 8% increases the NOx composition rate due to the high peak temperature.

INTRODUCTION

Nowadays, with increasing energy demand and tighter regulations, special care needs to be taken in energy production processes to increase efficiency and reduce pollutant emissions [1]. Traditional combustion techniques strike a balance between efficiency and pollutant emissions, especially NOx. Therefore, there is a need to find an alternative fuel that can fulfil the power required by the world. Biofuel is an ideal solution due to its environmentally friendly features and its flammable ability is comparable to standard gaseous fossil fuels [2]. Major advances in biogas processing and anaerobic waste management have taken place over the last 50 years. The most important area of research on biogas is the conversion of energy into an increased thermodynamically value by biogas [1,2]. Inert components constitute a large part of biogas and the heating value of this fuel is notably little, so biogas is known as a fuel with a low calorific value (LCV). As biogas is conventionally incinerated, ignition problems with regards to its constancy are found. As such, effective techniques are pursued to resolve these problems[3]. However, these two biogas drawbacks are spontaneously overcome by the use of flameless combustion technology, since flameless technology can operate adequately with significantly limited LVCs and in the oxy-fuel order. Besides, the removal of CO_2 from biogas is not necessary due to the flameless ability to combust CO_2. It can also be utilized in flameless combustion to lower the oxidizer [4,5]. Biogas produced naturally is a possible fuel substitute and a continuous and constant power provider in transportation and industrial boilers. Additionally, fertilizer and irrigation water is a by-

product of anaerobic digestion (AD) of natural waste materials[5]. Greater calorific values of biogas are attainable when the amount of methane (CH_4) is increased due to the removal of carbon dioxide (CO_2) from biogas ingredients. In certain users such as vehicle fuel, hydrogen sulfide (H_2S) and water vapour are eliminated from biogas entities because of the corrosive features [6]. LCV biogas is made up of flammable CH_4, non-flammable CO_2 as the fundamental entities and little concentrations of nitrogen (N_2), hydrogen sulfide (H_2S), carbon monoxide (CO), ammonia (NH_3), hydrogen (H_2), oxygen (O_2), water vapour (H_2O), dust and at times, siloxanes [7]. With regards to the calorific value of natural gas (36 MJ/m^3), the average calorific value of biogas is particularly little (around 21.5 MJ/m^3). Due to the numerous AD feedstock, CH_4 makes up approximately 40–80% of the biogas ingredients. As such, applying a lower CH_4 heating value at the conventional temperature and pressure (around 34,300 KJ/m^3), the heating value of biogas should be lesser at about 13,720–27,440 kJ/m^3. With a mixture of CH_4 and CO_2, in biogas greater than 98%, the physical characteristics are generally formed by these two gases. Table 1 shows the biogas components with regards to different feedstock [8].

.

TABLE 1. Composition of biogas [9]

Compound	Chemical Formula	Percentage (%)
Methane	CH_4	55 – 65
Carbon Dioxide	CO_2	35 – 45
Nitrogen	N_2	0 – 3ppm
Hydrogen Sulphide	H_2S	0 – 1ppm
Hydrogen	H_2	0 – 1ppm
Ammonia	NH_3	0 – 1ppm

Biogas has a lesser calorific value (LCV) of approximately 30 MJ/kg (60% CH_4) than that of pure methane at about 50 MJ/kg [10]. The combustion temperature of methane is around 645 ◦C and for biogas, approximately 700 ◦C [11]. There are a few techniques that can be utilized to enhance combustion and constancy, for instance, vortex and swirl flame. The first study on vortex flames was made by Gabler in 1998 [12] as shown in Fig. 1. Asymmetrical vortex combustor (AVC) is an innovative combustor model that can hold a constant flame over an extensive range of equivalence ratios [13]. The experiment made on ultra-reduced NO_X emissions was to investigate asymmetric compared to axisymmetric due to good mixing of air and fuel [14]. Despite the superior efficiency of flameless combustion with regards to fossil fuel use, different features of biogas flameless mode have not been thoroughly studied. Computer analysis is becoming more effective in its application because of its sufficient precision, affordability. As such, the various approach of biogas flameless combustion can be numerically studied. This research investigates a CFD model of biogas flameless combustion to decide the utmost crucial factors to consider in the biogas flameless regime Furthermore, the effects of hydrogen addition on the stability of combustion and emission.

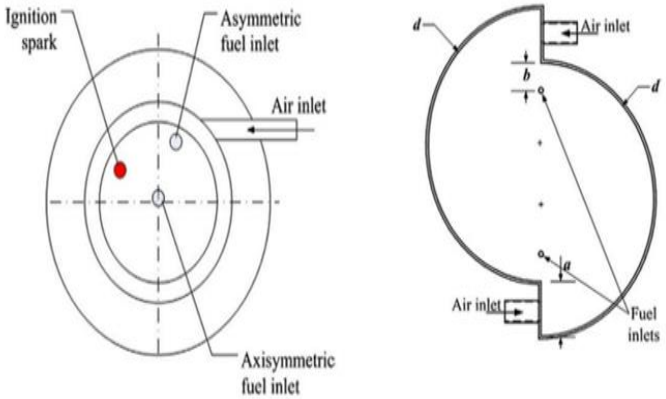

FIGURE 1. Schematic of the asymmetric vortex combustor reported by a) Gabler [12], b) Saqr [14].

METHODOLOGY

CFD MODELLING

The CFD developed for this numeral analysis relates to the geometry combustion of a previous study [12,14] and uses an asymmetric combustor with tangential air inlets and axial air and fuel inlets as shown in Fig. 2. The asymmetric vortex combustor has a dimension layout; a, b, R and L of 4, 4, 15 and 45 mm respectively. The fuel and air inlet nozzles had a= 1.5 mm diameter and circular cross-section. Exhaust gases exit the burner through a = 3mm diameter central outlet. Fig. 2 shows the asymmetric chamber design of the non-premixed forward air configuration. The design features six tangential air inlets and two axial fuels inlets and consists of two forward axial airflows. ANSYS 16 Modeller was utilized to fabricate the flameless burner, and ANSYS Meshing was utilized in netting the burner [15]. Mesh refinement, together with scalar characteristics, can be enhanced, and grid resolution can be ensured for stable flow. The number of mesh grids has a direct effect on the time it takes to solve a problem. The control volume meshes close to the air and fuel nozzles are tinier to improve the accuracy of predictions as shown in Fig. 3. Fig. 4 shows the plots of central axis temperature along with the axial position for four various meshes. M1 consists of 173,212 cells, while M2 consists of 200,282 cells. Tetrahedral elements were used to make M3=405,827 cells and M4=650,381 cells. Simulation data for different meshes when the preheated air temperature is set to 900K and the oxygen level of the oxidizer is set to 7%. The simulation results with M3=405,827 cells are good and agree with accurate and save time. The grid was tested independently in the emulation by converting the number of nodes to smaller meshes.

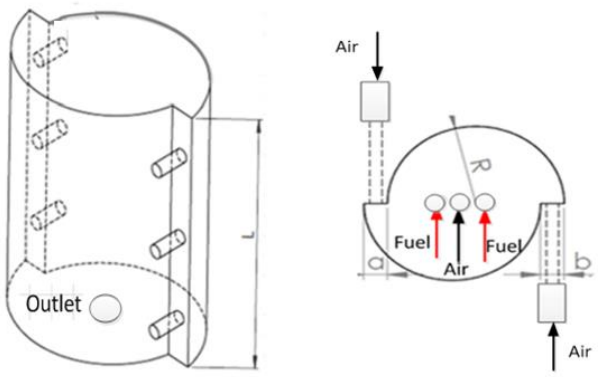

FIGURE 2. The design of mesoscale combustor flameless combustion (a) isometric view (b) top view.

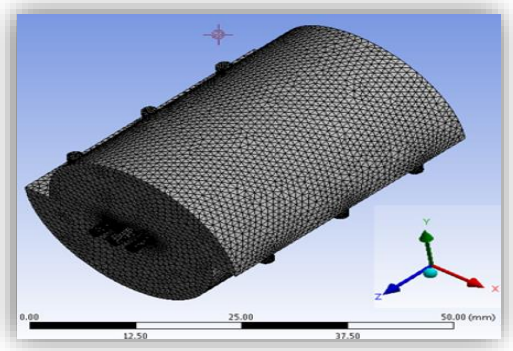

FIGURE 3. Mesh Meso-scale flameless combustion**.**

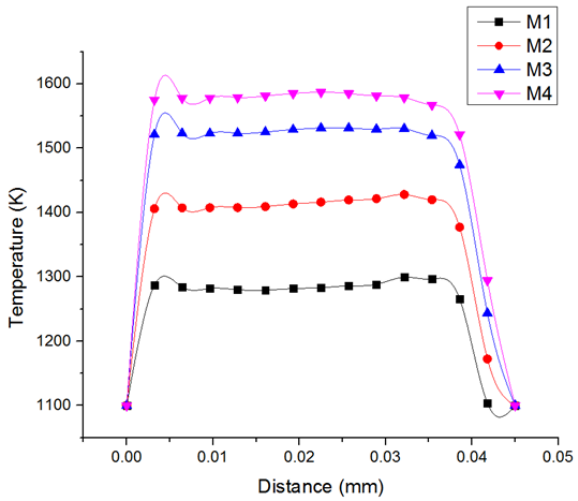

FIGURE 4. Grid independence test.

The CFD package ANSYS FLUENT16 [15] is used to dissolve the governing equations (transport equations such as continuity, energy, and momentum). The 3D conservation equations are given below for mass, momentum, and also energy [16–18]. The mass conservation is given as

$$u_i = \bar{u}_i + \acute{u}_i \quad (1)$$

$$\frac{\partial \rho}{\partial t} + \frac{\partial}{\partial x_i}(\rho u_i) = 0 \quad (2)$$

ρ and u_i are density and flow velocity in the i-direction respectively. The momentum equation is stated a

$$\frac{\partial \rho}{\partial t}\rho u_i + \frac{\partial}{\partial x_i}\rho u_i u_j = \frac{\partial p}{\partial x_j} + \frac{\tau_{ij}}{\partial x_i} + \rho \sum_{K=1}^{N} Y_K f_{K,j} \quad (3)$$

With the viscous tensor $\tau_{i,j}$ expressed as

$$\tau_{ij} = -\frac{2}{3}\ \mu \frac{\partial u_k}{\partial x_k}\ \delta_{ij} + \mu \left(\frac{\partial_{u_i}}{\partial_{x_j}} + \frac{\partial_{u_j}}{\partial_{x_i}}\right) \quad (4)$$

Where ρ, Y_k, $f_{k,j}$ stands for the pressure, the species *k* mass fraction, along with the volume force that acts on the j direction of the species (*k)* respectively, while δ_{ij} and μ indicates the Kronecker symbol and the dynamic viscosity respectively. The energy equation is given as:

$$\rho C_p \frac{DT}{Dt} = \dot{\omega}_T + \frac{\partial}{\partial x_i}\left(\lambda \frac{\partial T}{\partial x_i}\right) - \left(\rho \sum_{K=1}^{N} C_{P,k} Y_k V_k\right)\frac{\partial T}{\partial x_i} + \tau_{ij}\frac{\partial u_i}{\partial x_i} + Q +$$

$$\rho \sum_{K=1}^{N} Y_K f_{K,j}\ V_{kj} \quad (5)$$

Where variables C_p, *T*, and λ represent the mass heat capacity, the temperature, the thermal conductivity of the mixture, while $\dot{\omega}_T$,C_p ,*k*, and Q is the rate of heat release, the mass heat capacity of species k, and the heat source term.

$$\frac{\partial \rho Y_k}{\partial t} + \frac{\partial}{\partial x}(\rho(u_i + V_{k,i})Y_K) = \dot{\omega}_K \quad (6)$$

Where $V_{k,i}$ and $\dot{\omega}_K$ stands for the species *k* in the direction *i* and the reaction rate of species *k* diffusion velocity each. Assuming every species are fixed in the gas state, it can be conjected that the optimum gas behaviour is for all species. In this stable condition of the CFD model, biogas is used as the fuel while the equivalent ratio is variable of non-premixed flameless combustion mode. The equivalence ratio is used to determine whether a chemical reaction's fuel-air mixture is lean (Φ), stoichiometric (Φ = 1), or rich (Φ >1) [19]. In 300 K, the density of biogas, which contains 60% CH_4 and 40% CO_2 is 1.106 kg/m^3. while the density of CH_4 (100%) at the same temperature is calculated to be about 0.6682 Kg/m^3. Table 2 shows the densities of preheated air at varying temperatures and with different N_2 and O_2 mixtures. The general combustion reaction of biogas, with regards to the different mole fractions of CO_2, is shown in Eq. (7) [20].

$$(1-\beta)[(CH_4 + (2+x)(O_2 + 3.76N_2)] + \beta CO_2 \rightarrow CO_2 + 2(1-\beta) + H_2O + 7.56(1-\beta)N_2 + x(1-\beta)(O_2 + 3.76N_2) \quad (7)$$

Methane-air-2step is used to model the species transport and is calculated by the following equations [21].

$$CH_4 + {}^3\!/_2\, O_2 \rightarrow CO + 2H_2O \;\Delta G = -\frac{632.68\text{KJ}}{\text{mol}} \quad (8)$$

$$CO + {}^1\!/_{2O_2} \rightleftarrows CO_2 \quad \Delta G = -257.19\text{KJ/mol} \quad (9)$$

In the chemical reaction of equation (8) carbon monoxide (CO) and water vapour (H_2O) are produced, whereas equation (9) CO is oxidized to CO_2 and separation occurs. A chemical process for Combustion Chemistry Modelling consists of at least three segments: a gas-phase kinetic order (a collection of every wanted chemical reaction in simulation, among other things relevant Arrhenius coefficients), a thermodynamic database (thermodynamic coefficients of every gas-phase kinetic file), and a transport data order. The coefficients utilized in Eqs. (8) and (9) are the coefficients of the Arrhenius equation.

$$k = AT^{\beta} e^{-\left(\frac{E}{RT}\right)} \quad (10)$$

where *k* denotes reaction rate, *R* denotes a gas constant, *A* denotes pre-exponential, *T* denotes temperature and *β* denotes a dimensionless number of order one. The heat loss from the wall to the surroundings is also calculated by the equation. (11), Both thermal radiation and normal convective heat transfer are investigated [22]

$$q = h(T_{s,O} - T_\infty) + \varepsilon S(T^4{}_{s,o} - T^4{}_\infty) \quad (11)$$

where $T_{s,o}$ denotes the outer surface temperature, T_∞ denotes the ambient temperature set at 300 K, *h* denotes the natural convection coefficient with a deliberated constant value 5 W/m^2 K, σ = 5.67 x 10^{-8} W/m^2 K^4 denotes Stephane-Boltzmann constant and e denotes the solid surface emissivity.

According to previous studies on macro-scale flameless combustion technology, the dilution of oxidants is often referred to as one of the flameless formation fundamentals [23,24]. Studies made established that if the oxygen concentration in the combustion air rises to 15%, a flame is formed. The parameter for this experiment was chosen with regards to previous macro-scale flameless mode experiments. The oxidizer temperature in conventional combustion (21% O_2 and 79% N_2 by vol.) is 300 K, while the inlet oxidizer temperature in flameless combustion (case1: 5% O_2 and 95% N_2, case2: 7% O_2 and 93% N_2 by vol.) is 900 K, which is greater than methane's self-combusting temperature.

TABLE 2. air density (kg/m^3) in different temperatures.

Temperature (K)	5% O_2	7% O_2	9% O_2	10% O_2	21% O_2
300	1.146	1.15	1.152	1.154	1.177
500	0.687	0.689	0.691	0.692	0.7063
700	0.491	0.492	0.4937	0.4946	0.5046
900	0.382	0.383	0.3841	0.3847	0.3925

NUMERICAL CONDITIONS

Flameless oxidation, colorless dispersed combustion, moderate to extreme low oxygen Dilution (MILD) combustion, and high-temperature air combustion (HiTac) are all terms used to describe flameless combustion [9,25–28]. The CFD developed for this numerical analysis is based on the geometry combustion of a previous study by Saqr [14]. The simulations are focused on the flow field profile, temperature profile, and emissions of the combustor under biogas compositions at stoichiometric equivalence ratios (Φ=1). Synthetic biogas is made by mixing methane and carbon dioxide and adding various percentages of hydrogen to simulate biogas in various cases. In this analysis, a three-dimensional finite volume solver in FLUENT 16 is used for stable non-mixed combustion [15]. The spatial discretization of the mass, momentum, and energy transportation equations, is based on the upwind second-order scheme. In discrete momentum equations, the SIMPLE algorithm is utilized for combinations of pressure velocity [29]. The system was simulated using a two-step global process with the k–ε method as the viscous model and Eddy Dissipation Concept (EDC) as the turbulence chemistry interaction model [30,31]. Thermal NOx calculation uses the partial equilibrium model to predict the O radical concentration required. The boundary conditions are picked according to the previous macro-scale flameless mode experiments [32]. The running pressure and temperature are 0.5 bar and 300K respectively. The temperature of the inlet oxidizer (case1: 5% O_2 and 95% N_2, case2: 7% O_2 and 93% N_2, case3: 10% O_2 and 90% N_2 by vol.) is adopted in the Meso-flameless mode, 900 K, higher than the methane self-ignition temperature. The inlet temperature of CH_4 and biogas and the oxidizer is 300 K and the effects of the preheated oxidizer and fuel are (T_{inlet} = 300, 500, 700, 900 K), as well as the equivalence ratio (Ø= 1), was simulated to study the different aspects of combustion on NOx emission. Table 3 and 4, respectively, shows a description of the boundary conditions for the inlet oxidant and the boundary conditions for the fuel inlet, wall and pressure outlet with the general simulation shown in Table 5. For estimating the O_2 radical concentrations needed for thermal NOx prediction, partial equilibrium models were applied. In consecutive iterations, if the residual in each equation is less than $1x10^{-6}$, the solution is considered to be converged which was carried out applying grid independence tests. M3=305,729 cells with a minimum cell size of 0.003 mm per grid independence test as shown in Fig. 3.

TABLE 3. The boundary condition of inlet oxidant

Oxidizer inlet	Value
Temperature	$T_{inlet\ air}$ = 300 K
Gauge Pressure	0
Hydraulic diameter	2mm
Turbulent intensity	10
Oxygen concentration	7%
Density (ρ) Kg/m^3	ρ= 1.16 kg/m^3

TABLE 4. The boundary condition of fuel inlet, wall and pressure outlet

	Boundary conditions	
Fuel inlet	Temperature	$T_{inlet\ fuel}$ = 300
	Gauge pressure	0
	Hydraulic diameter	3
	Turbulent intensity	10
	Fuel	CH_4
	Density	0.6682 Kg/m^3
	Mass flow rate	Variable
Wall	Wall slip	Non-slip
	Material	Steel
	Heat transfer confection	5 $w/m^2 k$
Pressure outlet	Hydraulic diameter	3mm
	Gauge pressure	0
	Turbulent intensity	5

TABLE 5. Initial Settings of simulation

Steps	
Viscous model	k–e Standard
Radiation model	Discrete ordinate (DO)
Combustion model	Species transport / partially premixed combustion
Mixture properties	Methane–air
Turbulence chemistry interaction	EDM Volumetric
Reaction	Thermal NOx
NOx	Prompt NOx

RESULTS

EFFECT VARIOUS OF FUEL COMBUSTION ON TEMPERATURE DISTRIBUTION COMBUSTION

The temperature profiles that have been recorded along the central axis of the burner was demonstrated in Fig. 5 and Fig. 6 during CH_4 traditional combustion and biogas flameless combustion. The temperature of the flameless mode of biogas in the entire burner is lower than the traditional burning of CH_4 and biogas [23,33]. However, the temperature of traditional combustion varied from one part to another part of the chamber during combustion and hot spots can be created without difficulty. While the temperature inside the burner was regular in flameless combustion about 1100 K. This state offers an optimal situation for reducing the formation of NOx. Besides, fuel usage drops from 3.56 g/s in traditional combustion with biogas to 1.23 g/s in a flameless setup. The raised concentration of CO_2 that passes through the combustion burner regulated the combustion reactions that reduce the temperature of the chamber. Due to its high heat capacity (C_p) at raised temperatures, CO_2 also has superior cooling effects and its improved radiation properties made it easier to take in greater radiation from the reaction area. These conditions lowered the device temperature at the walls of the room. The findings are consistent with studies that were carried out by Szegö et al [34]and Dally et al. [35]. Thus, the key advantages of biogas flameless combustion are hot spot removal and the temperature constancy within the flameless chamber and low emission [9]. Reciprocally, a temperature peak towards the burner occurred in conventional combustion with methane as according to previous studies [33]. A temperature uniformity ratio within the burner was defined by Yang et al [36] to measure the temperature uniformity as follows.

$$R_u = \sqrt{\sum \left(\frac{T - \bar{T}}{\bar{T}} \right)^2} \qquad (12)$$

All the registered temperatures of the horizontal axes in the centre of the burner were used to test Ru in this simulation, and Ru was equal to 0.04. Where Ru is a ratio of temperature constancy, the T(K) denotes all points of the burner which was measured temperature and $\bar{T}$ is the temperature average. In flameless combustion, since the difference between T and $\bar{T}$ is very small at any point of the burner Ru should tend to zero.

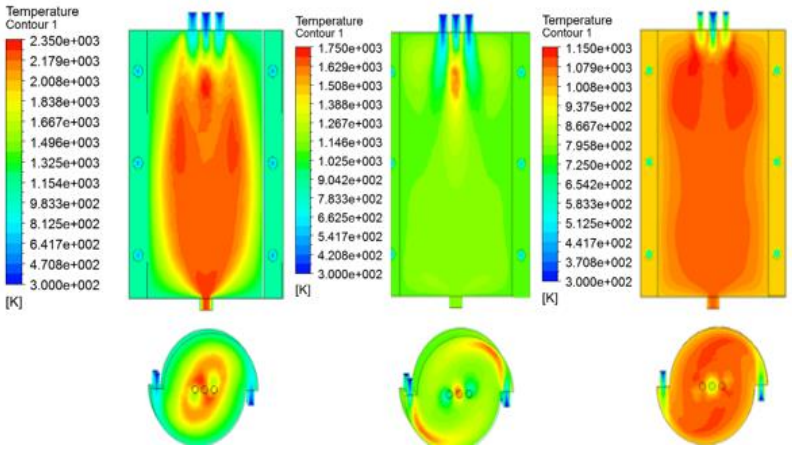

FIGURE 5. Show temperature of **(a)** CH_4 conventional, **(b)** Biogas conventional combustion and (c) biogas flameless combustion at equivalence ratio Φ=1.

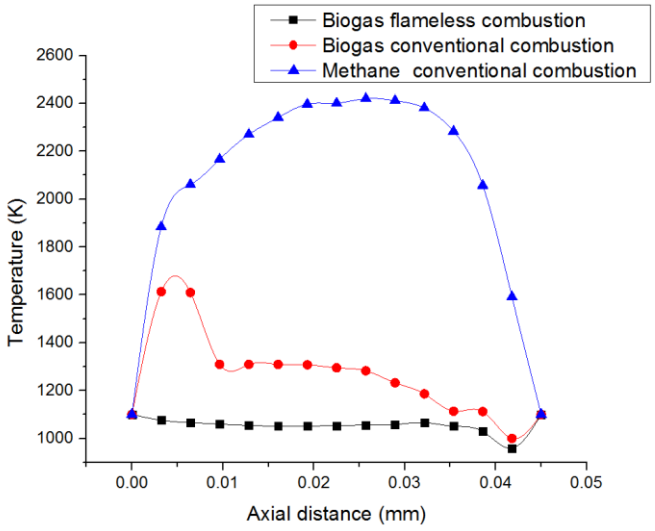

FIGURE 6. The temperature characteristics at the central axis of the combustor of CH_4 conventional combustion, biogas conventional combustion and biogas flameless combustion at equivalence ratio Φ=1

EFFECT VARIOUS 0F BIOGAS COMBUSTION ON EMISSION

The gas analyzer results indicate that in biogas flameless combustion as opposed to traditional combustion, the flameless mode significantly decreased the formation of contaminants**.** Fig. 7 illustrates the formation of NOx emission of biogas flameless mode, traditional biogas combustion and traditional methane burning within the Centre of the axis of the combustion chamber. Pollutant concentration records show that, because of the significant conditions of the flameless combustion, the flameless mode is increasingly vulnerable to NOx reduction as compared to conventional combustion [23,33]. In flameless combustion, NOx formation is suppressed. Certain factors including significantly high temperature, the constitution of hot spots within the combustion furnace, resident time and great concentrations of oxygen in the combustion reaction, play an important part in the formation of thermal NOx based on the Zeldivich formulation [37]. According to Fig. 6, the temperature within the burner is lesser and regular in flameless mode, relative to conventional combustion. The key causes of low NOx formation are the constant temperature within the flameless chamber and the consequent avoidance of hot spot formation, high reactant velocity and low oxygen concentration [38–40]. In other words, thermal NOx is removed using flameless combustion, but other inconspicuous NOx production regimes, such as prompt NOx and N_2O intermediate NOx, remain [41–43]. Besides, Fig. 7 depicts the flow of NOx production in traditional methane combustion by raising the temperature and the rate of oxidizer. It can be inferred that having greater exposure to air and preheated air temperature improves the rate of NOx production in a methane traditional combustion.

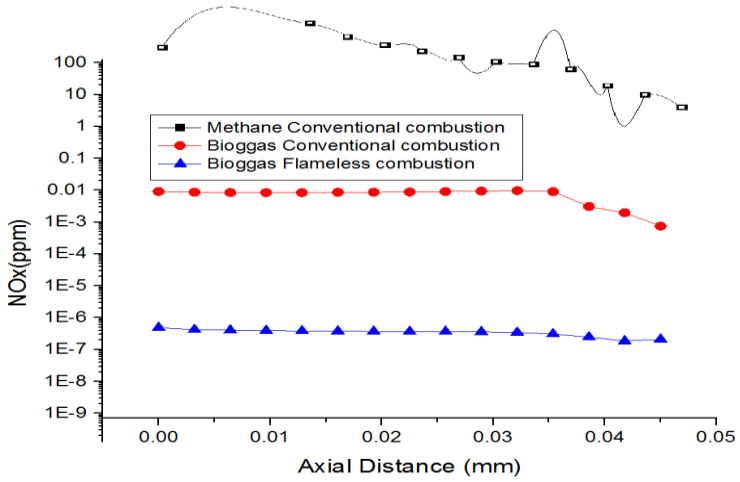

FIGURE 7. The NOx emission profiles along the central axis of the combustor of CH_4 conventional combustion, biogas conventional combustion and biogas flameless combustion at equivalence ratio Φ=1.

Fig. 8 shows that the concentration of biogas flameless O_2 is very low and uniform along the axis of the furnace. The diluted oxidizer in a thorough fast blending procedure in the biogas flameless technique is responsible for the low O_2 concentration. Aside from that, the flameless chamber's uniform temperature, which is greater than that of the biogas auto ignition, ensures a constant setting for the creation of the biogas flameless system. The little amount of OH radical concentration that governs CO conversion to CO_2, is responsible for the high CO concentration in the flameless regime [5,34]. Fig. 9 shows the CO concentration along the centerline at a stoichiometric condition for different compositions. biogas conventional combustion showed the lowest CO concentration. In contrast, compositions of biogas flameless mode higher CO concentrations but at a comparable level biogas conventional combustion [33]. For this combustor, CO emission is high near the bottom of the combustor but drops to almost a constant value of about 200 ppm of CO at around the 0.045 mm axial position. This could be due to further oxidation of CO to CO_2 in flameless mode [33,34].

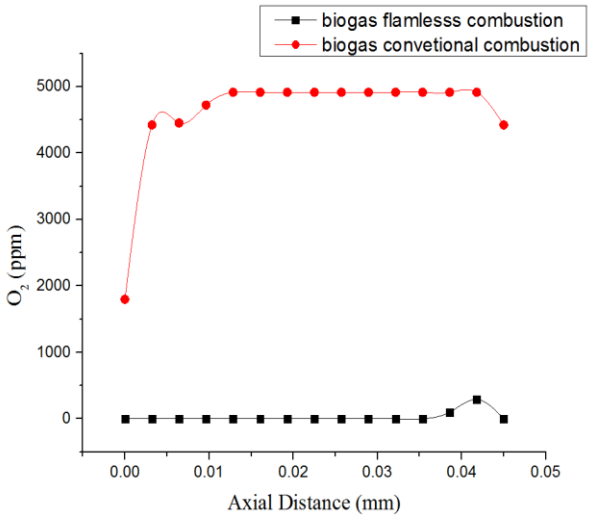

FIGURE 8. The O_2 emission characteristics at the central axis of the combustor of biogas conventional combustion and biogas flameless combustion at equivalence ratio Φ=1.

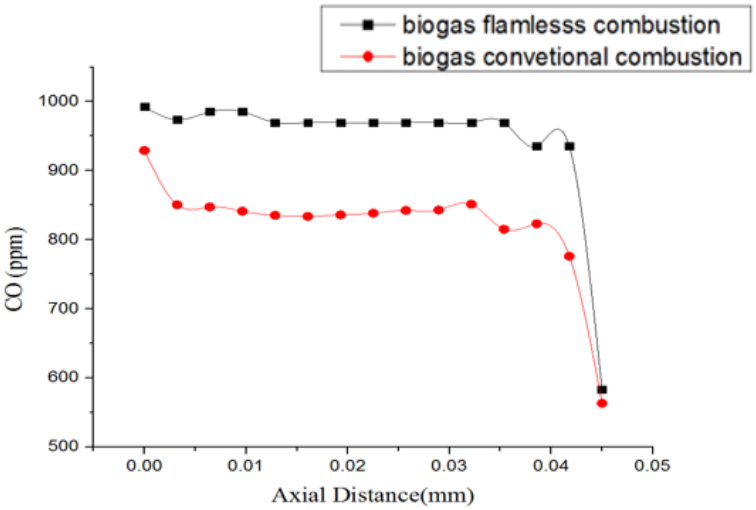

FIGURE9. The CO emission characters at the central axis of the combustor of biogas conventional combustion and biogas flameless combustion at equivalence ratio Φ=1.

Fig. 10 and 11 depicts the concentrations of CH_4 and CO_2 along the biogas spray combustor's central axis. Since CH_4 and CO_2 account for 60% and 40% of biogas, respectively. Due to the high peak temperature values in the traditional configuration, very high concentrations of CO_2 and CH_4 have been observed in biogas conventional combustion. Due to CO_2 Comprise 40% of biogas components, the temperature of the reactants is lowered. Consequently, hot spots which play a decisive role in NOx and CO_2 formation are eliminated due to low conversion of CO to CO_2 in flameless mode [5,33]. However, the concentration of CH_4 and CO_2 decreases sharply in biogas flameless mode compared to conventional combustion [23]. In flameless mode, this ensures that the combustion phenomenon happens uniformly throughout the burner.

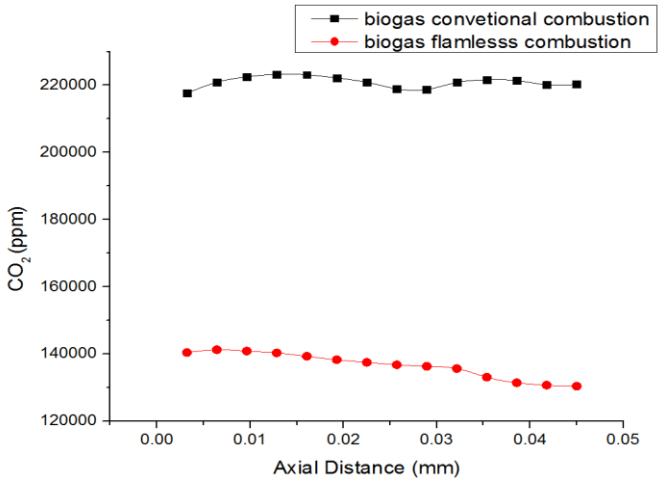

FIGURE 10. The CO_2 emission characteristics at the central axis of the combustor biogas conventional combustion and biogas flameless combustion at equivalence ratio Φ=1.

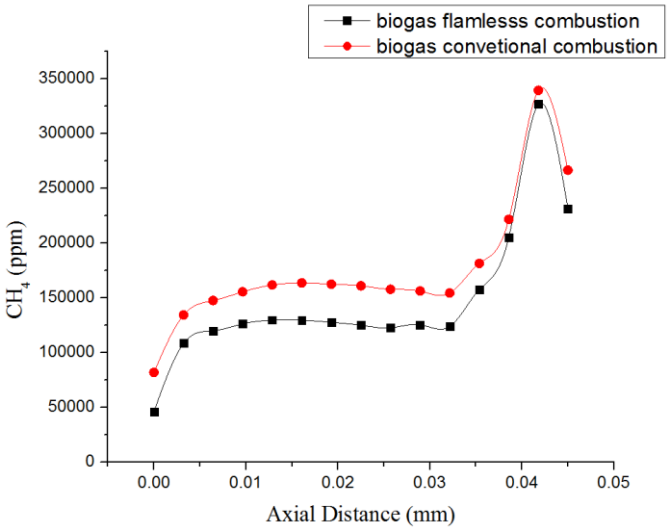

FIGURE 11. The concentration of CH_4 at the central axis of the combustor of biogas conventional combustion and biogas flameless combustion at equivalence ratio Φ=1.

Fig. 12 depicts the species' streamline in both traditional and flameless combustion. Due to the turbulence environment, the mixture of the fuel and oxidizer species in a flameless regime is completed faster than in a traditional regime leading to ultra-low emission [23,44]. The dilution of the oxidizer, as well as the complete and rapid mixing procedure, are also responsible for the low concentration of O_2 in the flameless mode [45,46].

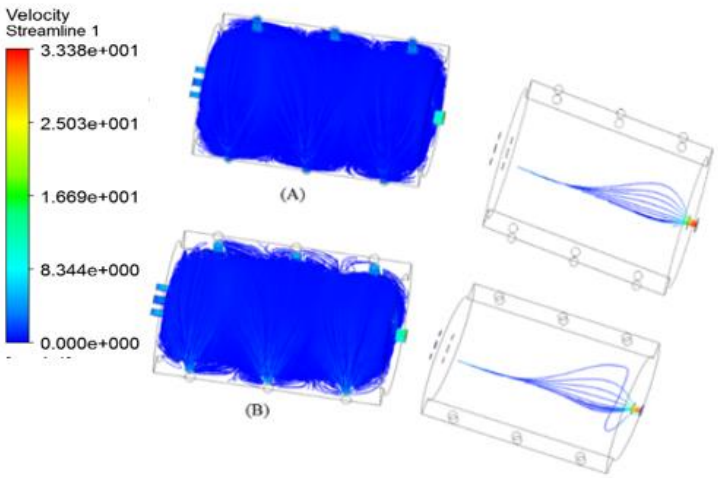

FIGURE 12. The streamline species of biogas (A) biogas conventional combustion (B) flameless combustion.

BIOGAS CONVENTIONAL COMBUSTION WITH PREHEATED AIR

The average temperature of conventional preheated combustion rises within the chamber because of the increased enthalpy of preheated air, results in the significant lowering of fuel intake. Fig. 13 depicts the results of preheated air temperature on fuel intake in conventional combustion. While Preheated conventional combustion can help reduce fuel usage, NOx production rises when combustion is greatly preheated [47,48]. This is because thermal NOx increases rapidly at high temperatures, this effect is due to a rise in the combustor's peak temperature [49]. Fig. 14 (a) and (b) show the different maximum temperatures within the combustor and NOx production in both conventional and flameless preheated combustion concerning the preheated oxidizer temperature. It can be inferred that preheated conventional combustion of biogas is unable to raise the internal temperature of the combustor substantially. Nevertheless, obvious differences are observable at peak temperature and NOx production in CH_4 preheated conventional combustion.

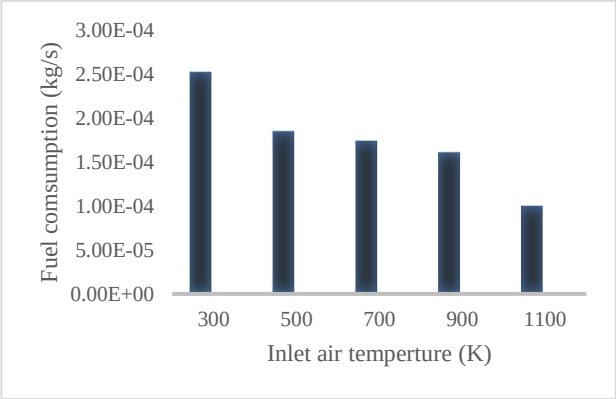

FIGURE 13. The results of air preheating temperature on fuel usage in conventional combustion

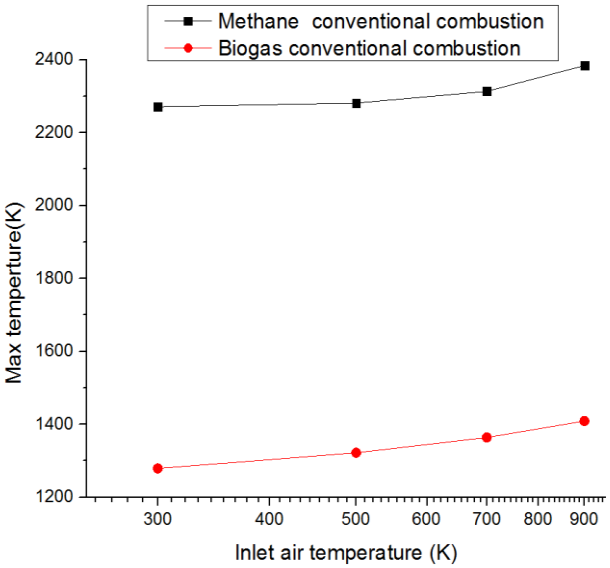

(A)

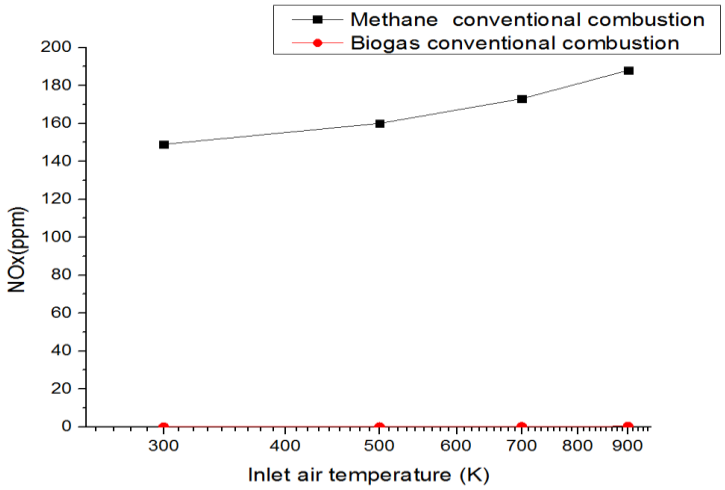

(B)

FIGURE 14. (A) The differences of maximum temperature in conventional and flameless preheated combustion. (B) NOx production in conventional and flameless preheated combustion.

FLAMELESS COMBUSTION OF BIOGAS

In this simulation, the oxygen concentration in the oxidizer is assumed to be 5%, 7%, 9%, and 10% by volume, respectively, and the oxidizer is diluted by N_2. Fig. 15 demonstrates the flameless constitution in the combustor when the mass flow rate and equivalent ratios of the air and fuel inlets remain constant at 2.7652×10-6 kg, 5.65985×10-7 kg/s and (Φ=1) respectively, $T_{inlet\text{-}oxidizer}$ = 900 K. Data generated to show that increasing the concentration of oxygen with a steady mass flow rate increases the temperature gradient. The result obtained is similar to the findings generated by [45,50] Consequently, NOx emissions increase as the combustion temperature increases as shown in Fig. 16. So, oxygen concentration exhibited a significant role in establishing flameless combustion. it observed high NOx

emissions at increase O_2 concentrations at a constant temperature of 300 K as shown in Fig. 17. As result, It was observed with an increase in oxygen concentration resulted in increases in temperature of combustion, which leads to increases in NO_X emission as according to results [23,45,50]. The enthalpy required for biogas auto-ignition temperature is provided by the preheated oxidizer [45]. In biogas flameless combustion, the average temperature of the burner is lower than in ordinary CH_4 combustion in a room [23]. Conventional combustion has very high and fluctuating temperatures as compared to biogas flameless combustion with uniform temperatures. As a result, in flameless mode, hot spots that play a critical role in NOx formation are removed. The temperature of the reactants reduces because CO_2 accounts for 40% of the biogas components. It is due to CO_2 high heat capacity, particularly at high temperatures [33]. So, in biogas flameless combustion, the wall temperature of the combustor is lower than CH_4 traditional combustion and biogas traditional combustion throughout the burner about1030 K as shown in Fig. 18. The ratio of uniformity in the flameless burner is measured at about zero using the mathematics formula for temperature uniformity ratio Yang et al [36]. This situation is also perfect for protecting the material of the burner and reducing NOx formation. Furthermore, in flameless mode, fuel consumption drops from 3.56 g/s in traditional biogas combustion to 1.23 g/s.

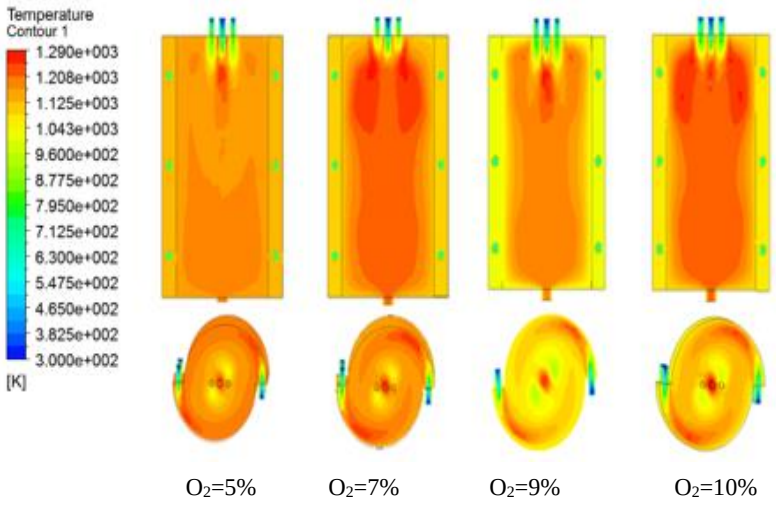

FIGURE 15. Biogas flameless combustion production with different oxygen concentrations.

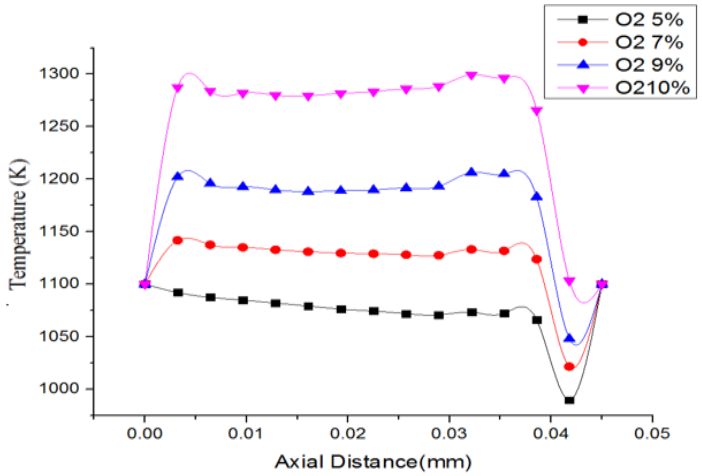

FIGURE 16. Effect Oxygen concentration (%) on the central temperature profile

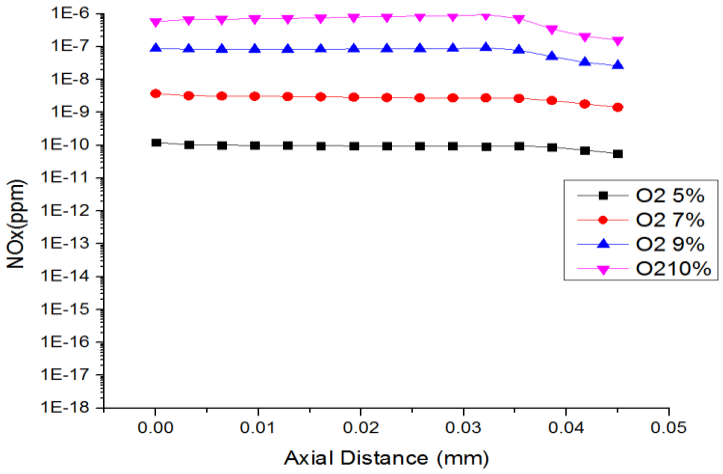

FIGURE 17. Effect Oxygen concentration (%) on the central NOx emission profile.

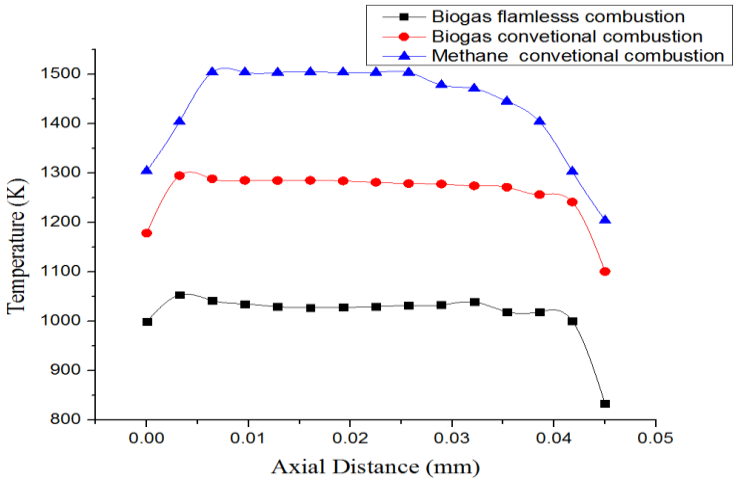

FIGURE 18. Temperature distribution of Wall.

EFFECTS OF HYDROGEN ADDITION TO BIOGAS COMPONENTS ON TEMPERATURE AND NOX EMISSION

Since the density of fuel decreases when hydrogen is added to the biogas composition, the flow rate of fuel must be increased to ensure a stoichiometric ratio case. The structure of biogas flameless mode changes when added hydrogen is applied to the components leads to the increased temperature rises in a combustor. Fig.19 indicates the temperature inside the combustor in each of the four simulation images with hydrogen changes. Fig. 20 also shows the effects of hydrogen addition on the biogas component in axial temperature distribution in a flameless combustor mode. It was discovered that only 2% hydrogen added to the biogas components ensured the flameless biogas regime's stability and temperature uniformity within the furnace. When the hydrogen content of biogas exceeds 2%, the peak temperature of flameless combustion increases. In a flameless combustion regime, adding hydrogen to the biogas ingredient improves combustion stability while increasing pollutant formation [5,51]. Furthermore, as more hydrogen is added, the density of biogas changes, and the fuel combination's flow rate increases. The higher temperature is due to the larger specific energy content of hydrogen-enriched biogas, as well as lower radiation losses due to lower carbon dioxide production [52].

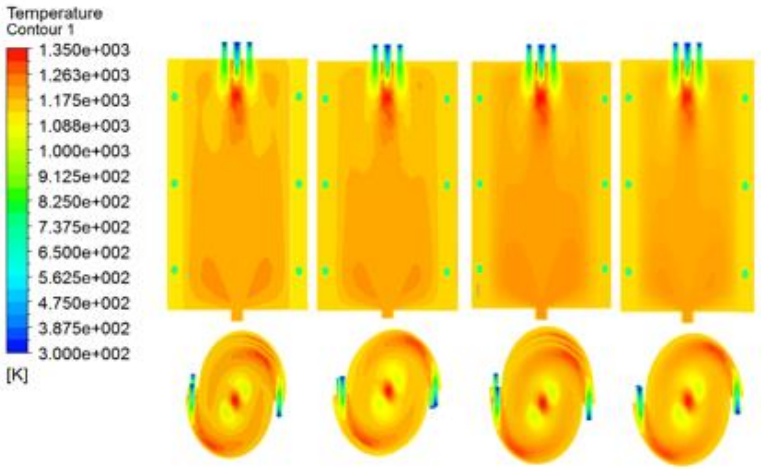

H_2= 2% H_2= 4% H_2= 6% H_2= 8%

FIGURE 19. Effect H_2 concentration (%) on temperature distribution in a combustor.

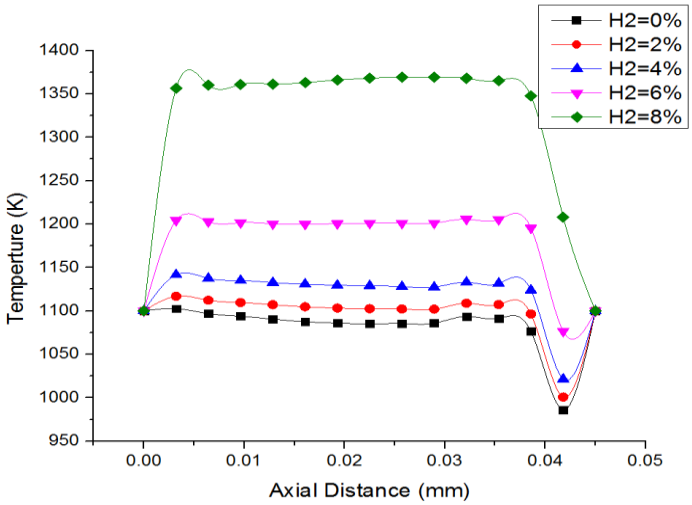

FIGURE 20. Effect H_2 concentration (%) on the central temperature profile.

Fig. 20 and 21 show the NOx composition and the effects of hydrogen content on NOx formation in biogas flameless combustion respectively. When H_2 (up to 4%) is utilized to the biogas flameless mode, the NOx formation rate decreases in this graph. However, as the H_2 rate increases (from 4% to 8%) in the biogas content, the proportion of the NOx composition intensifies. Adding hydrogen to the biogas flameless combustion component increases pollutant production while improving combustion stability [5]. The oxygen concentration in the flameless combustor is shown in Fig 22 under different conditions. The levels of oxygen concentration in H_2 and H_4 is lower than that of flameless biogas combustion. As a result, low levels of NOx formation in biogas with low levels of hydrogen may be expected. As a result, though adding hydrogen to biogas can be beneficial, the amount should be carefully monitored since biogas–hydrogen mixtures increase NOx emissions [3,51].

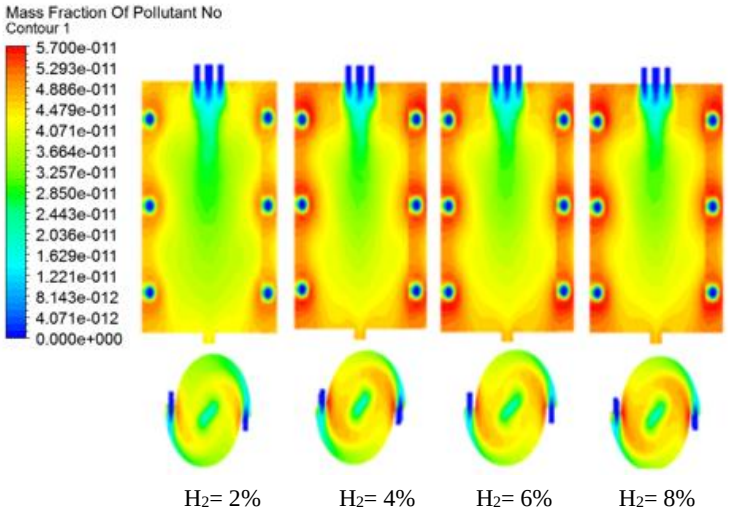

FIGURE 20. NOx formation Distribution in the combustor

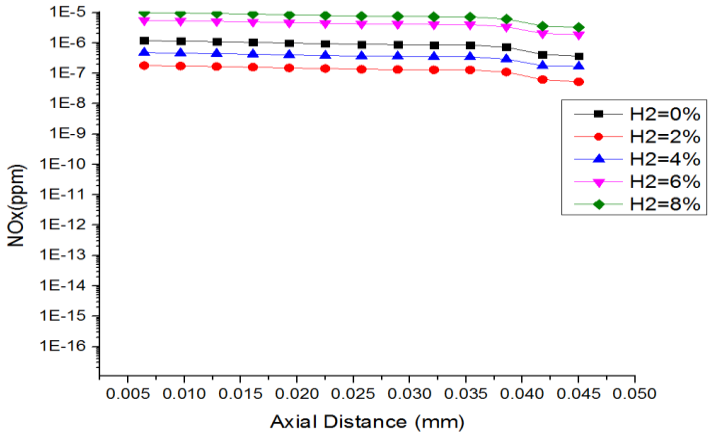

FIGURE 21. Effect H_2 concentration (%) on the central NOx emission profile.

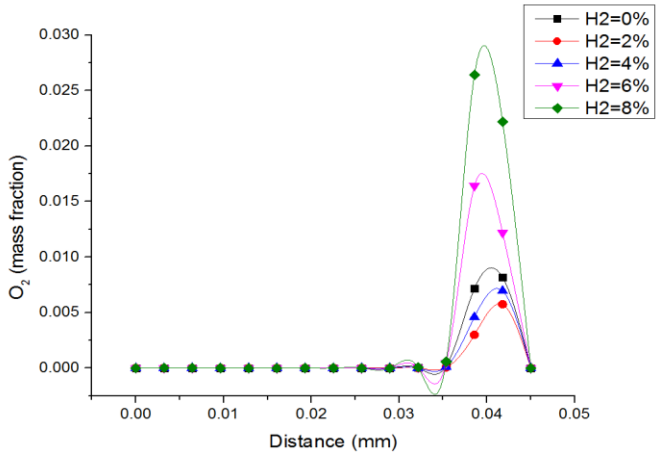

FIGURE 22. Hydrogen - Oxygen Concentration of Enriched Biogas Flameless Combustion

CONCLUSION

The combustion characteristics of the biogas flameless regime were investigated using computational fluid dynamics. The basic k–e formulation was used to simulate the two-step reaction scheme because of its precision and robustness for a wide range of turbulent flows. The biogas has a low calorific value (LCV), it is necessary to utilize a high calorific value fuel to preheat the burner to achieve biogas auto-ignition temperature. The results of preheated temperature on conventional combustion that were examined showed that in preheated biogas conventional combustion, fuel usage lowered but NOx production rose significantly. In the flameless combustion technique, energy loss is reduced because the temperature within the chamber and the temperature of the walls are regular. The streamlines of flameless modes suggest that biogas combustion is more turbulent than conventional combustion. In the flameless regime, the mixture of fuel and oxidant is completed faster than in the conventional regime due to the turbulent environment and full biogas combustion in the zone close to the burner is completed. In addition, the low concentration of O_2 in flameless combustion contributes to the dilution of the oxidizer and the complete and fast mixing process. The CO and NOx formation was found to be extremely poor of biogas combustion. The biogas flameless combustion has a higher efficiency than conventional combustion. Due to heat recovery, heat given off from emissions in biogas flameless combustion was lesser than in the conventional system. Indeed, biogas flameless products with a high CO_2 species concentration have a higher heat capacity and improved radiation heat transfer in the system. Just 2% hydrogen applied to the biogas components was found to be sufficient to ensure the flameless biogas regime's stability and temperature uniformity within the burner. When the hydrogen content of biogas exceeds 4%, the peak temperature of flameless combustion increases. However, adding hydrogen above 4% increases the NOx composition rate due to the high peak temperature. In a flameless combustion regime, adding hydrogen to the biogas ingredient improves combustion stability while increasing pollutant formation.

NOMENCLATURE

LCV	Low Calorific Value
CFD	Computational Fluid Dynamics
AD	Anaerobic digestion
3D	A three-dimensional
q	Heat transfer (KW)
k	Reaction rate

REFERENCE

1. S. E. Hosseini and M. A. Wahid, “Feasibility study of biogas production and utilization as a source of renewable energy in Malaysia,” *Renew. Sustain. Energy Rev.,* 19 (x) 454–462 (2013).
2. S. E. Hosseini and M. A. Wahid, “Necessity of biodiesel utilization as a source of renewable energy in Malaysia,” *Renew. Sustain. Energy Rev.,* 16 (8) 5732–5740 (2012).
3. C. Jeong, T. Kim, K. Lee, S. Song, and K. Min, “Generating efficiency and emissions of a spark-ignition gas engine generator fuelled with biogas – hydrogen blends,” *Int. J. Hydrogen Energy,* 34 (23) 9620–9627 (2009).
4. S. Chen and C. Zheng, “Counterflow diffusion flame of hydrogen-enriched biogas under MILD oxy-fuel condition,” *Int. J. Hydrogen Energy,* 36 (23) 15403–15413 (2011).
5. S. E. Hosseini and M. A. Wahid, “Development of biogas combustion in combined heat and power generation,” *Renew. Sustain. Energy Rev.,* (40) 868–875 (2014).
6. P. Gupta, R. S. Singh, A. Sachan, A. S. Vidyarthi, and A. Gupta, “Study on biogas production by anaerobic digestion of garden-waste,” *Fuel,* 95 (x) 495–498 (2012).
7. G. Taleghani and A. S. Kia, “Technical-economical analysis of the Saveh biogas power plant,” *Renew. Energy,* 30 (3) 441–446 (2005).
8. M. Hagen *et al.*, “Adding Gas from Biomass to the Gas Grid.,” (7) 1- 144 (2001).

9. S. E. Hosseini, M. A. Wahid, and A. A. A. Abuelnuor, “Biogas Flameless Combustion : A Review,” *Appl. Mech. Mater.*, 388, 273–279 (2013).
10. A. Noyola, J. M. Morgan-Sagastume, and J. E. López-Hernández, “Treatment of biogas produced in anaerobic reactors for domestic wastewater: Odor control and energy/resource recovery,” *Rev. Environ. Sci. Biotechnol.*, 5 (1) 93–114 (2006).
11. W. Baader, E. Dohne, and M. Brenndörfer, “Biogas in Theorie und Praxis Behandlung organischer Reststoffe aus der Landwirtschaft durch Methangärung,” *KTBL-Schrift*, 229, 2–4 (1978).
12. H. C. Gabler, *An experimental and numerical investigation of asymmetrically-fueled whirl flames* . (1998).
13. K. M. Saqr., “Aerodynamics and Thermochemistry of Turbulent confined Asymmetric Vortex Flames. A thesis submitted in fulfillment of the requirements for the award of the degree of Doctor of Philosophy (Mechanical Engineering),”)(4) 1-226 (2011).
14. K. M. Saqr, H. S. Aly, M. M. Sies, and M. A. Wahid, “Computational and experimental investigations of turbulent asymmetric vortex flames,” *Int. Commun. Heat Mass Transf.*, 38 (3) 353–362 (2011).
15. “‘ANSYS Fluent Theory Guide Release 16.0, SAS IP.’ Inc 89- 895(2015)
16. K. M. Saqr, H. S. Aly, M. A. Wahid, and M. M. Sies, “Numerical simulation of confined vortex flow using a modified k-ε turbulence model,” *CFD Lett.*, 1 (2) 87–94 (2009).
17. K. M. Saqr, H. S. Aly, H. I. Kassem, M. M. Sies, and M. A. Wahid, “Computations of shear driven vortex flow in a cylindrical cavity using a modified k-ɛ́ turbulence model,” *Int. Commun. Heat Mass Transf.*, 37 (8) 1072–1077 (2010).
18. M. M. Sies and M. A. Wahid, “Numerical investigation of the asymmetrical vortex combustor running on biogas,” *J. Adv. Res. Fluid Mech. Therm. Sci.*, 74 (1) 1–18 (2020).
19. S. . Turns, *Turns SR. An Introduction to Combustion Concepts and Applications.* (2013).
20. C. Cohé, C. Chauveau, I. Gökalp, and D. F. Kurtuluş, “CO_2 addition and pressure effects on laminar and turbulent lean premixed CH_4 air flames,” *Proc. Combust. Inst.*, 32, 1803–1810 (2009).
21. F. L. Dryer and C. K. Westbrook, “Simplified Reaction Mechanisms for the Oxidation of Hydrocarbon Fuels in Flames,” *Combust. Sci. Technol.*, 27 (1–2) 31–43 (1981).
22. G. Bagheri, E. Hamidi, M. A. Wahid, A. Saat, and M. M. Sies, “Effects of CO_2 dilution on the premixed combustion of CH_4 in micro combustor,” *Appl. Mech. Mater.*, 388, 251–256 (2013).
23. S. E. Hosseini, G. Bagheri, and M. A. Wahid, “Numerical investigation of biogas flameless combustion,” *Energy Convers. Manag.*, 81, 41–50 (2014).
24. B. Danon, E. S. Cho, W. De Jong, and D. J. E. M. Roekaerts, “Numerical investigation of burner positioning effects in a multi-burner flameless combustion furnace,” *Appl. Therm. Eng.*, 31 (17–18) 3885–3896 (2011).
25. M. Katsuki and T. Hasegawa, “The science and technology of combustion in highly preheated air,” *Symp. Combust.*, 27 (2) 3135–3146 (1998).
26. I. B. Özdemir and N. Peters, “Characteristics of the reaction zone in a combustor operating at mild combustion,” *Exp. Fluids*, 30 (6) 683–695 (2001).
27. J. A. Wuenning and J. G. Wuenning, “Flameless Oxidation to Reduce Thermal {NO}-formation,” *Prog. Energy Combust. Sci.*, 23, 81–94 (1997).
28. V. K. Arghode and A. K. Gupta, “Development of high intensity CDC combustor for gas turbine engines,” *Appl. Energy*, 88 (3) 963–973 (2011).
29. S. V. Patankar and D. B. Spalding, “A calculation procedure for heat, mass and momentum transfer in three-dimensional parabolic flows,” *Int. J. Heat Mass Transf.*, 15 (10) 1787–1806 (1972).
30. J. P. Kim, U. Schnell, and G. Scheffknecht, “Comparison of different global reaction mechanisms for MILD combustion of natural gas,” *Combust. Sci. Technol.*, 180 (4) 565–592 (2008).
31. B. F. Magnussen and B. Hjertager, “On mathematically modeling with special emphasis on soot formation and combustion,” 16 (8)719–729 (1977).
32. S. E. Hosseini and M. A. Wahid, “Enhancement of exergy efficiency in combustion systems using flameless mode,” *Energy Convers. Manag.*, 86, 1154–1163 (2014).
33. S. E. Hosseini and M. A. Wahid, “Biogas utilization: Experimental investigation on biogas flameless combustion in lab-scale furnace,” *Energy Convers. Manag.*, 74, 426–432 (2013).
34. G. G. Szegö, B. B. Dally, and G. J. Nathan, “Operational characteristics of a parallel jet MILD combustion burner system,” *Combust. Flame*, 156 (2) 429–438 (2009).
35. B. B. Dally, E. Riesmeier, and N. Peters, “Effect of fuel mixture on moderate and intense low oxygen dilution combustion,” *Combust. Flame*, 137 (4) 418–431 (2004).
36. W. Yang and W. Blasiak, “CFD as applied to high temperature air combustion in industries furnaces,” *IRFR*

Combust. J., (11) 2–4 (2006).
37. A. A. Nizami and N. P. Cernansky, "kinetics of pollutant formation and destruction in combustion," *Symp. Combust.*, 17 (1) 475–483 (1979).
38. G. M. Choi and M. Katsuki, "Advanced low NOx combustion using highly preheated air," *Energy Convers. Manag.*, 42 (5) 639–652 (2001).
39. M. Flamme, "Low NOx combustion technologies for high temperature applications," *Energy Convers. Manag.*, 42 (15–17) 1919–1935 (2001).
40. S. Seepana and S. Jayanti, "Flame structure and NO generation in oxy-fuel combustion at high pressures," *Energy Convers. Manag.*, 50 (4) 1116–1123 (2009).
41. S. E. Hosseini, S. Salehirad, M. A. Wahid, M. M. Sies, and A. Saat, "Effect of diluted and preheated oxidizer on the emission of methane flameless combustion," *AIP Conf. Proc.*, 1440, 1309–1312 (2012).
42. I. D. Bedoya, S. Saxena, F. J. Cadavid, R. W. Dibble, and M. Wissink, "Experimental study of biogas combustion in an HCCI engine for power generation with high indicated efficiency and ultra-low NOx emissions," *Energy Convers. Manag.*, 53 (1) 154–162 (2012).
43. C. Galletti, A. Parente, M. Derudi, R. Rota, and L. Tognotti, "Numerical and experimental analysis of NO emissions from a lab-scale burner fed with hydrogen-enriched fuels and operating in MILD combustion," *Int. J. Hydrogen Energy*, 34 (19) 8339–8351 (2009).
44. C. Ghenai and I. Janajreh, "Combustion of Renewable Biogas Fuels," *J. Energy Power Eng.*, 9, 831–843 (2015).
45. M. Mehregan and M. Moghiman, "A numerical investigation of preheated diluted oxidizer influence on NOx emission of biogas flameless combustion using Taguchi approach," *Fuel*, 227 (7) 1–5 (2018).
46. S. Komonhirun and P. Yongyingsakthavorn, "Effects of mesh type on a non-premixed model in a flameless combustion simulation," (2018).
47. M. A. Wahid and S. Ehsan Hosseini , "Utilization of Biogas Released from Palm Oil Mill Effluent for Power Generation Using Self- preheated Reactor," Energy Convers. Manag., 105 (8) 957–966 (2015).
48. A. Sarkar and U. K. Saha, "Role of global fuel-air equivalence ratio and preheating on the behaviour of a biogas driven dual fuel diesel engine," *Fuel*, 232(6) 743–754 (2018).
49. S. E. Hosseini, M. A. Wahid, A. Abdeen, and A. Abuelnuor, "High Temperature Air Combustion : Sustainable Technology to Low NOx Formation," *Int. Rev. Mech. Eng.*, 6, 947–954 (2012).
50. A. A. Abuelnuor, M. A. Wahid, H. A. Mohammed, and A. Saat, "Flameless combustion role in the mitigation of NOx emission : a review," *Int. J. ENERGY Res.*, 38 (x) 827–846 (2014).
51. S. E. Hosseini, G. Bagheri, M. Khaleghi, and M. A. Wahid, "Study on the characteristics of hydrogen-enriched biogas co-flow flameless combustion," *Recent Adv. Mech. Mech. Eng. Conf.*, 52–61 (2015).
52. M. Ilbas, "The effect of thermal radiation and radiation models on hydrogen-hydrocarbon combustion modelling," *Int. J. Hydrogen Energy*, 30 (10) 1113–1126 (2005).